Probing Astroparticle and Particle Physics at the Pierre Auger Observatory: highlights and perspectives

Antonella Castellina[1], for the Pierre Auger Collaboration[2]

1 Osservatorio Astrofisico di Torino (INAF), Torino and INFN, Sezione di Torino, Italy
2 Full author list: https://www.auger.org/archive/authors_2024_07.html
E-mail: spokespersons@auger.org

*22nd International Symposium on Very High Energy Cosmic Ray Interactions (ISVHECRI 2024)
Puerto Vallarta, Mexico, 8-12 July 2024*

Abstract

With more than 15 years of data acquisition, the results from the Pierre Auger Observatory provide the most precise data on ultra-high energy cosmic rays (UHECRs) in the world. It is now beyond doubt that the UHECR composition becomes lighter for energies increasing up to ~ 2 EeV, and it starts getting heavier above this energy when approaching ultra-high energies. A predominantly extragalactic origin of UHECRs beyond the ankle is proven with high significance, while at higher energies there are indications of correlation with nearby sources. The collected data allow us to study the properties of hadronic interactions at ultra-high energies and test the existence of possible effects beyond the Standard Model of particles. The future prospects opening up with the Auger-Prime upgrade are described.

1 Introduction

Ultra-high energy cosmic rays, defined as cosmic particles of energy greater than $\sim 10^{17}$ eV, have been studied since the second half of the 20th century, when they were first observed in experiments like Volcano Ranch and Haverah Park. Their detection is based on an indirect technique, which exploits the extensive air showers produced when these particles interact with atmospheric nuclei. Two different techniques were used in the past, exploiting either surface detectors measuring the lateral and time distribution of secondary particles at the ground or fluorescence telescopes, which collect the UV light emitted by the shower in the Earth's atmosphere [1].

The Pierre Auger Observatory [2], whose construction started back in 2004, is currently providing the largest sample of ultra-high energy events ever collected. The Observatory has been conceived as a hybrid one, in that it is equipped with two kinds of detectors: a grid of 1600 water-Cherenkov stations deployed over an area of 3000 km^2, at 1500 m mutual

distance (the Surface Detector, SD-1500) and 24 fluorescence telescopes overlooking this area from 4 different sites (the Fluorescence Detector, FD). Two inner areas have been instrumented with surface detector stations spaced 750 m and 433 m apart respectively (SD-750 and SD-433) to extend the measurements to lower energies. These detectors are overlooked by three additional high-elevation fluorescence detectors.

Data are collected by the SD with a duty cycle of almost 100%, while the FD can operate only during dark and moonless nights, reaching a duty cycle of ∼15%. Exploiting the sample of hybrid events, those measured by both the SD and the FD, it is possible to obtain an almost completely data-driven energy calibration. The calorimetric energy determined by the FD, corrected for the so-called invisible energy carried away by neutrinos and muons [3], can in fact be correlated to an SD energy estimator (the particle density at 1 km from the shower core, corrected by the attenuation), thus providing a calibration which can then be applied to all the events detected by the SD. The FD energy resolution amounts to about 8% and the overall systematic uncertainty on the energy scale is 14% [4].

The scientific achievements of the Pierre Auger Collaboration cover different and complementary fields of research. The search for the origin of UHECRs is based on the measurement of the energy spectrum and mass composition of the primaries, on extensive anisotropy searches on both large and intermediate angular scales, and on studies of neutral messengers, photons and neutrinos. In addition to astrophysical studies, it is possible to explore the characteristics of hadronic interactions at energies unattainable at human-made accelerators, and to look for hints of physics beyond the Standard Model, such as possible violations of Lorentz invariance, or signals of super-heavy dark matter. The results obtained at the Pierre Auger Observatory led to major advances in our understanding of the properties of UHECRs, providing a global view which appears to be much more complex than the one proposed in the past.

2   Experimental results

Arrival directions - Although the angular distribution of the arrival directions of the UHECRs appears to be nearly isotropic, large-scale anisotropies can be looked for focussing on scales much larger than the angular resolution, where the cumulative flux from multiple objects could possibly be detected despite the magnetic deflections suffered by the charged UHECRs.

A large-scale dipolar anisotropy was detected for energies above 8 EeV [1] [5], and further explored in [6]. Thanks to a huge exposure of $123,000$ km^2 sr yr, the significance of the established equatorial dipole for the cumulative energy bin above 8 EeV is now 6.8σ, and for energies between 8 and 16 EeV it is 5.7σ [7]. The corresponding flux is shown in the left panel of Fig.1. The dipole direction points ∼115° away from the Galactic centre, clearly indicating the extragalactic origin of these UHECRs. The dipole amplitude is found to increase with energy, as expected due to larger relative contribution that arises at high energies from nearby sources, that are more anisotropically distributed than the integrated flux from the distant ones, which is furthermore strongly attenuated due to the interactions of cosmic rays with the background radiation. The observed dipolar anisotropy and its evolution with energy appear to be compatible with the local large-scale distribution of matter, assuming that the sources emit UHECRs with a mixed composition. Possible quadrupolar moments have been looked for, but they are not found to be statistically significant.

Hints of intermediate-scale anisotropy have been obtained at higher energies, for which the deflections of UHECRs due to magnetic fields are expected to be small enough. The most significant excess from an all-sky blind search is found above 38 EeV in a top-hat angular region with radius 27° in the region of CenA. In the right panel of Fig.1, the corresponding local

---

[1]1 EeV = 10^{18} eV.

Li-Ma significance is shown in Galactic coordinates. Exploiting catalog-based searches, the most significant results are the overdensities in the Centaurus region and the hints of correlation with starburst galaxies [8], with a post-trial p-value now increased to 6.6×10^{-5} [9]. Combining vertical and inclined events collected with the SD, the field of view of the Pierre Auger Observatory covers all declinations up to $\delta \leq 44°.8$, allowing us a partial coverage of the regions where the Telescope Array reported excesses in their data [10]. After correcting the energy thresholds for the known mismatch between the energy scales of the two observatories [11], with comparable statistics, we have not found any significant results.
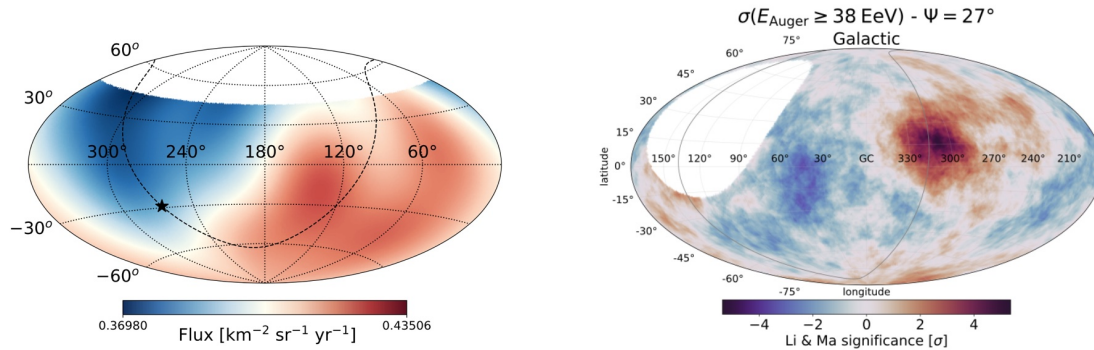
Figure 1: Left: Flux above 8 EeV, with a top-hat smoothing radius of 45°, equatorial coordinates. The star shows the Galactic Center, the dashed line indicates the Galactic Plane [7]. Right: local Li-Ma significance at $E \geq 38$ EeV within a top-hat window of 27° radius, Galactic coordinates. The supergalactic plane is shown as a gray line. The blank area is outside the field of view of the Pierre Auger Observatory [9].

Energy spectrum and mass composition - Together with the study of arrival directions, the evaluation of the UHECRs energy spectrum and nuclear composition provides information about the characteristics of the possible sources, and the injection and escape of these nuclei in the intergalactic space, also allowing us to test our knowledge of the background radiation and magnetic fields they encounter during propagation. In the top panel of Fig.2, we show the energy spectrum obtained by combining two different spectra, measured with SD-750 and SD-1500 [12, 13]. They are compatible within systematic uncertainties, which are taken into account in the combination. The resulting spectrum covers a huge range, from ~ 100 PeV, with partial coverage of the second knee [14], up to the highest energies, clearly showing the ankle and the flux suppression, at $(4.8 \pm 0.1 \pm 0.8)$ EeV and $(47 \pm 3 \pm 6)$ EeV respectively. Thanks to the large exposure, an additional inflection at $\simeq 14$ EeV, the instep, was unveiled for the first time.

The nuclear mass of the UHECRs cannot be determined directly; the most reliable information on UHECR composition comes from the measurement of the depth of shower maximum, X_{max}. The first two moments of the X_{max} distributions obtained in different analyses are shown in the bottom panels of Fig.2, and compared to the predictions for proton- and Fe-initiated air shower simulations using post-LHC hadronic interaction models [15]. The most precise $\langle X_{max} \rangle$ and $\sigma(X_{max})$ are obtained from the direct measurement of the longitudinal distribution of the showers by the FD [17], but they are prone to the limited duty cycle. To exploit the 100% duty cycle of the SD, data-driven methods based on the analysis of the risetimes of the recorded signals were used in [16], confirming the FD results. More recently, the SD measurements have been extended to the highest energies, exploiting machine learning algorithms [18]. The results are further confirmed by a completely independent measurement performed with the AERA radio array of the Pierre Auger Observatory [19].

While different post-LHC hadronic interaction models predict a constant elongation rate of ~ 60 g cm^{-2} per decade of energy for primaries with the same nuclear mass, the data show a
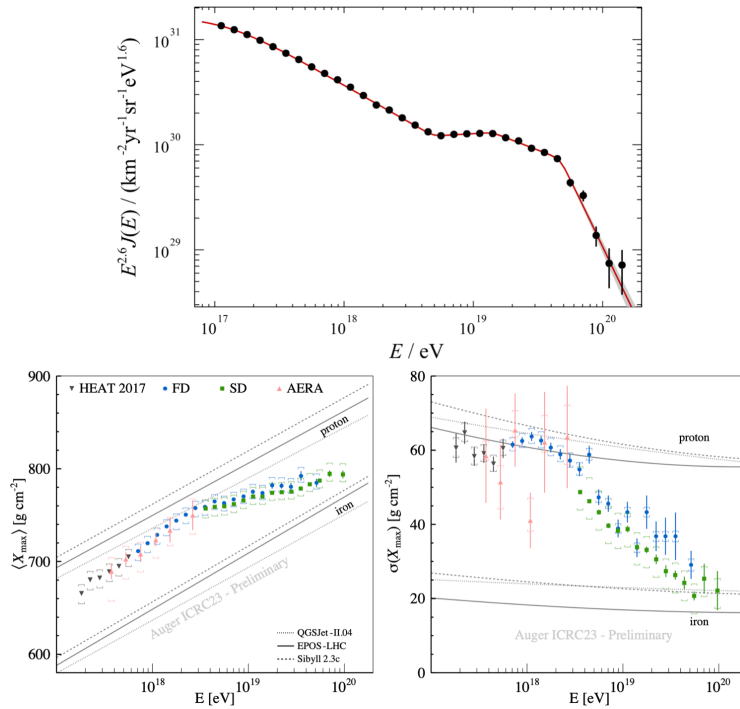
Figure 2: Top: the UHECR energy spectrum after combining the individual measurements by the SD-750 and the SD-1500 scaled by $E^{2.6}$. The best fit model is shown by the red line [12,13]. Bottom: the first two moments of the $X_{\max}$ distributions measured by the HEAT, FD, SD and AERA [15].

larger increase of $77\,\mathrm{g\,cm^{-2}}$ per decade of energy up to about 2 EeV, clearly indicating that the mean primary mass is getting lighter up to this energy. On the contrary, the mean mass turns to heavier above this energy, with an elongation rate of $26\,\mathrm{g\,cm^{-2}}$ per decade of energy.

The shower-to-shower fluctuations and the dispersion in mass of the primary beam are the two ingredients of $\sigma(X_{\max})$. Its evolution with energy confirms the previous conclusion: the large values at low energy show that the primaries are either light or a mixture of light nuclei, whereas a small value of $\sigma(X_{\max})$ corresponds to purer intermediate or heavy composition.

Thanks to the large increase in statistics when using the data collected by the SD, it is possible to study the structure of the $\langle X_{\max} \rangle$ evolution with energy, shown in Fig.3. While a nice agreement is found with the result from the FD when fitting it above 2 EeV with a constant slope, the best fit is obtained with a 3-breaks model. The kinks appear correlated to the features of the energy spectrum outlined above.

The composition fractions measured at Earth can be obtained by fitting templates of $X_{\max}$ distributions for different masses (p, He, CNO, Fe) generated by simulations based on post-LHC hadronic interaction models [15]. The result of this study is shown in Fig.4; an alternating dominance of increasingly heavier masses is visible. The flux is dominated by light primaries above 1 EeV; since no significant anisotropy is visible at these energies in the direction of the Galactic plane, these primaries must be extragalactic. The proton fraction appears to be very low at the highest energies, although no information is available from FD above the suppression region.

Astrophysical interpretation - Astrophysical models of increasing complexity have been put forward to describe the energy and composition features of UHECRs measured at Earth. A good description of the data was obtained starting from a simple model in which stationary and uniform sources from two extragalactic populations inject several nuclear components and only propagation is taken into account [20]. The low energy one appears to have a quite
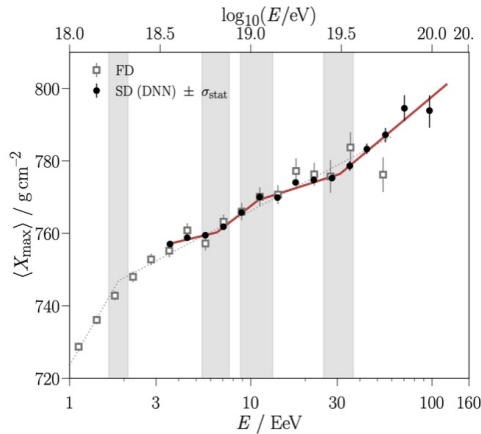
Figure 3: Evolution of $\langle X_{max}\rangle$ as a function of energy for the SD (black) and the FD (grey) [18,22]. The grey regions indicate the uncertainties in the energy of the identified breaks in the $\langle X_{max}\rangle$ evolution.
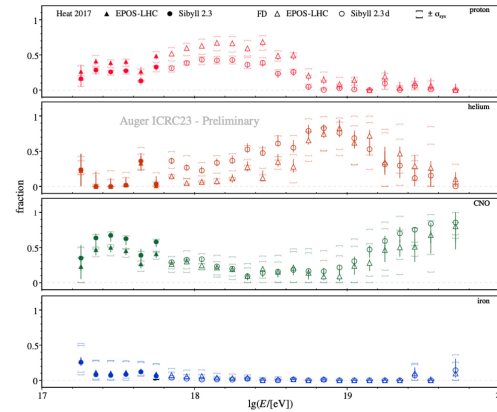
Figure 4: Fits of the fractions of masses in the UHECR flux. The X_{max} distributions measured by the FD have been fit using templates of pure mass distributions generated using post-LHC hadronic interaction models.

soft spectrum at the escape and a mix of protons and intermediate-mass nuclei, in agreement to the composition fractions derived from the X_{max} distributions [21], while sources above the ankle emit a mixed composition with a hard escape spectrum and a low rigidity cutoff. The partial contributions to the energy spectrum and the corresponding relative mass abundances at Earth are shown in Fig.5. In this scenario, the instep feature around 10 EeV appears to derive from the interplay between He and CNO mass groups injected at the sources, whose flux is shaped by the propagation. Our data indicate a predominance of the maximum energy reach at the sources over the GZK cutoff as the cause of the suppression.

The expected cosmogenic neutrino flux associated to the best-fit results appears to be entirely provided by the low energy component; in fact, the contribution of the high energy component is negligible due to its quite low rigidity cutoff. A comparison with the best current upper limits on neutrinos, obtained at the Pierre Auger Observatory above 0.1 EeV [23], allows a strong evolution of the low-energy population to be excluded. The power of multi-messenger analyses in getting information about the properties of UHECRs sources has been further explored in [24]. In the more realistic scenario of a discrete source distribution, the presence of
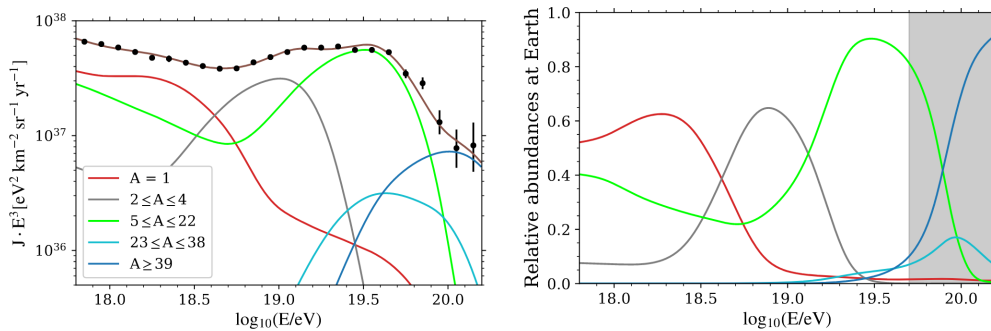
Figure 5: Partial contributions to the energy spectrum at the top of the atmosphere grouped according to mass number (left) and the corresponding relative abundances as a function of the energy (right), assuming a propagation-only scenario with two extragalactic populations [20].

extragalactic magnetic fields between the closest sources and the Earth can affect the shape of the spectrum of cosmic rays at Earth. The flux of low-rigidity particles is reduced; this magnetic horizon effect can thus provide an alternative explanation for the hardness of the high-energy population spectrum [25], although requiring large inter-source separations and

large magnetic field RMS amplitude in the Local Supercluster. The combined fit was refined, limited to the region above the ankle, by taking into account also the arrival directions of the UHECRs, whose distribution, as discussed above, indicates a potential correlation with nearby sources. In this case, the best fit is obtained with a model containing a flux fraction of around 20% from the starburst galaxy catalog at 40 EeV, with a hard, nitrogen-dominated injection spectrum [26].

3 UHECRs at the particle physics frontier

Hadronic interactions - The models of hadronic interactions that are used to interpret the measured observables in terms of mass composition are based on extrapolations of many parameters obtained at accelerators at energies below $\sqrt{s} = 13$ TeV for pp collisions and in a kinematic region covering pseudorapidities below 5 for charged particles, very different from the characteristics of hadronic interactions in air showers. Tests on the predictions of the models in the UHE region have been performed in the Pierre Auger Observatory in different analyses.

The p-Air cross-section was measured for the first time at $\sqrt{s} = 57$ TeV [27]; based on this result, the stability of the mass composition fits presented above was checked with respect to allowed changes in the p-p cross-section [21].

A deficit in the number of muons predicted at different levels by all models was demonstrated
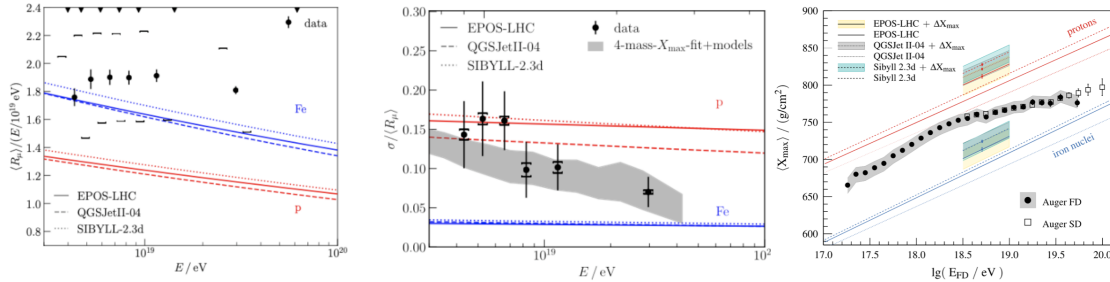
Figure 6: Left: average muon content $\langle R_\mu \rangle$ per shower energy E as a function of the shower energy [28]. Middle: measured relative fluctuations in the number of muons as a function of the energy, compared to the predictions for proton (red) and iron (blue) showers. Grey band: expectation from the measured mass composition [31]. Right: measured energy evolution of $\langle X_{\max} \rangle$. Shaded bands: expectations from the modified $X_{\max}$ scales. Lines: original unmodified model predictions for p and Fe initiated showers [32].

by various independent studies of the muon content in air showers above 0.1 EeV [28–30]. An example of the result obtained with inclined showers (which are almost purely muonic, as the electromagnetic component is quickly absorbed in the atmosphere) is shown in the left panel of Fig.6. The change of slope in data with respect to models suggests a transition from light to heavier masses as the energy increases; a 30% to 80% increase in the relative muon number would be needed to match the measurement. A study of the relative fluctuations in the muon number [31] indicates that the post-LHC models describe well the fluctuations of the energy partition in the first interaction up to ultra-high energies, as shown in the middle panel of Fig.6. This result excludes strong deviations in the first interaction, suggesting that a small effect accumulating over many generations could instead be invoked to increase the muon number.

A recent test on the predictions of the models has been performed [32], limited to the energy region between 3 and 10 EeV. The analysis is based on allowing modifications of both $X_{\max}$ and SD signals scales in the simulations; indeed, a wrong $X_{\max}$ evaluation in Monte Carlo

would cause an incorrect estimate of the muon number, being it directly related to the primary mass through $N_\mu \propto A^{1-\beta}$ [33]. Monte Carlo templates of the 2-dimensional distributions of (S_{1000}, X_{max}) have been used to fit the experimental distributions. The best fit is obtained by allowing a deeper X_{max}, by about 20 to 50 g cm^{-2}, and an increased hadronic signal, by about 15% to 25%. In the right panel of Fig.6, the modified predictions on the $\langle X_{max} \rangle$ elongation rate between 3 and 10 EeV are shown in comparison with the measurements. As a consequence of the modified scales, smaller uncertainties on the estimated fractions of different primary nuclei are obtained due to the reduced difference among the models.

Beyond the standard model - UHECRs provide excellent means to study the possible existence of effects beyond the Standard Model of particle physics. Non-standard mechanisms, like departures from relativity such as Lorentz invariance violation (LIV), can result in a perturbative modification of the particle dispersion relation $E_i^2 = p_i^2 + m_i^2 + \sum_{n=0}^{\infty} \delta_i^{(n)} E_i^{n+2}$ (where i=type of particle, n=approximation order).

The ultra-high energy and the extremely large propagation path of these particles make them the ideal candidates to search for these effects, expected to be suppressed at low energies and for short travel distances. The presence of LIV can be searched for looking for changes in the propagation of UHECRs [34] or in the air shower development in the atmosphere [35]. In the first case, the energy threshold of photo-hadronic interactions can be modified by the LIV; depending on the composition of the UHECRs, the attenuation length of photo-meson production or photo-disintegration may become extremely large and suppress particle interaction during propagation in the extragalactic space. A comparison of the expected spectrum and composition at the top of the atmosphere with the measured ones can thus provide limits to the allowed level of violation. In particular, assuming the scenario which best fits our data on spectrum and composition [20] with the addition of a sub-dominant proton component, limits of $\delta_\gamma^{(1)} \sim 10^{-40}$ eV^{-1} and $\delta_\gamma^{(2)} \sim 10^{-60}$ eV^{-1} can be derived for n=1 and n=2 respectively.

Considering only the case $p \ll M_{Planck}$, the modified dispersion relation can be written as $E_i^2 = p_i^2 + m_i^2 + \eta_i^{(n)} E_i^{2+n}/M_{Planck}^n$. Due to the presence of the LIV in the development of air showers, if the parameter $\eta < 0$, the probability of decay of the π^0 can decrease till the particle becomes stable. A growth of the hadronic cascade is then expected, with a subsequent increase in the production of muons and a decrease of the electromagnetic component, with the effect of moving the X_{max} to shallower depths. The relative fluctuation in the number of muons as a function of energy for different levels of LIV between 10^{-3} and 10^{-15} is shown in the left panel of Fig.7. Using a mixed initial composition of protons and iron, a lower bound of $\eta^{(1)} > -5.95 \times 10^{-6}$ can be derived at 90.5% CL.
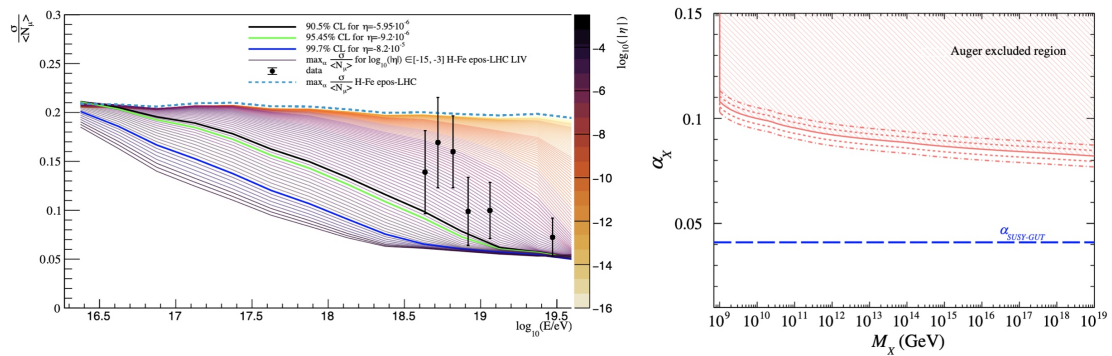
Figure 7: Left: Relative muon fluctuations as a function of energy, for different parametrizations [35]. The standard case is shown by the black line, while the coloured ones indicate different violation strengths. Right: 95% CL upper limits on the coupling constant α as a function of the mass M_X of a dark matter particle X [36].

In many models, super-heavy particles, relics of the early Universe, have been proposed to form the dark matter. They can decay through instanton-induced processes producing a UHE flux of photons, neutrinos and hadrons. The strongest constraint on the SHDM comes from photons, as the huge exposure accumulated at the Pierre Auger Observatory has enabled us to reach sensitivities to photon fluxes less than few percent of that of UHECRs. Primary photons produce air showers that can be distinguished from hadronic ones thanks to their characteristics: the energy transfer to the hadronic channel is reduced, making them muon-poor and the small multiplicity of the electromagnetic interactions causes the shower to develop deeper in the atmosphere. The search for photon primaries has been conducted with different and independent analyses [23]; no candidate photon has been found in a large energy range, from ~ 0.2 EeV up to about 40 EeV. The lifetime of the X particle can be related to the coupling constant α_X according to the relation $\tau_X \sim M_X^{-1} \exp(4\pi/\alpha_X)$. Exploiting the limits placed on the flux of UHE photons at the Pierre Auger Observatory, values of the dark-sector gauge coupling greater than about 0.09 can be ruled out, as shown in the right panel of Fig.7 [36]. In a similar way, it is possible to constrain the mixing angle between sterile and active neutrinos for SHDM masses larger than 10^8 GeV [37].

4 Conclusion and outlook

Fundamental advances in understanding ultra-high-energy cosmic rays have been reached thanks to the data collected at the Pierre Auger Observatory. The results discussed above show that UHECRs have a complex and increasingly heavier mass composition, a fact confirmed by the non-observation of cosmogenic neutrinos and photons. The transition from a galactic to an extragalactic origin takes place below the ankle, as supported by the mixed composition getting lighter above the 2nd knee up to 2 EeV and by the smooth transition from isotropy to a dipolar anisotropy above a few EeV. The combined analysis of the UHECR energy spectrum and mass composition fits a scenario in which heavier and heavier mass groups take over, with increasing purity. The energy spectrum is shaped by the interplay of the different mass groups, and its suppression above ~ 45 EeV appears to be mainly attributed to the exhaustion of the sources. Besides the observation of the dipolar anisotropy above 8 EeV, hints of correlation have been found with the direction of starburst galaxies and active galactic nuclei, although not yet at the level of identifying individual sources.
Hadronic interaction models have been tested in an energy and kinematic region unattainable by the human-made accelerators; the most recent analyses point to the need to shift both the modelled $X_{\max}$ and signal scales to reconcile them to the data in the ankle region. At the particle physics frontier, the existence of physics beyond the standard model could be tested.

The new perspectives opened by the current results called for an upgrade of the Observatory, known as AugerPrime [38], whose main aim is the collection of new information about the primary mass of the highest energy cosmic rays on a shower-by-shower basis with high statistics. The deployment of AugerPrime is completed, its key elements including a 3.8 m^2 Surface Scintillator Detector (SSD) and a 30 to 80 MHz radio detector (RD) above each of the water-Cherenkov stations of the SD. A new upgraded unified board allows us to process the signals at 120 MHz, with increased local trigger capabilities and timing accuracy improved to 2 nsec. Thanks to a fourth small photomultiplier inserted in each station, non-saturated signals can be measured up to distances as close as 250 m from the shower core. Underground muon detectors are being co-located with the stations of the SD-433 and SD-750 to directly measure the muon content of air showers. The upgraded Observatory will enable powerful analyses based on the exploitation of multi-hybrid measurements provided by the different detectors. Combined evaluation of $X_{\max}$ with the scintillators and the water-Cherenkov stations

will provide more precise information on the UHECR composition up to the highest energies, thus allowing us to perform mass-based anisotropy searches; 5σ significance in the correlation with starburst galaxies can be obtained in five years from now. Better constraints on cosmogenic photons and neutrinos will be set thanks to the increased statistics and the development of new dedicated triggers. After completion of the current commissioning phase [39–43], the upgraded Pierre Auger Observatory, AugerPrime, will start collecting new data and perform multi-messenger studies for ten more years.

References

[1] M. Nagano, A.A. Watson, *Observations and implications of the ultrahigh-energy cosmic rays*, Rev.Mod.Phys. **72**, 689 (2000).

[2] A. Aab et al. (Pierre Auger Coll.), *The Pierre Auger Cosmic Ray Observatory*, Nucl. Instrum. Meth. A **798**, 172 (2015), doi:10.1016/j.nima.2015.06.058

[3] A. Aab et al. (Pierre Auger Coll.), *Data-driven estimation of the invisible energy of cosmic ray showers with the Pierre Auger Observatory*, Phys.Rev. D **100**, 082003 (2019), doi:10.1103/PhysRevD.100.082003

[4] B. Dawson (Pierre Auger Coll.), *The energy scale of the Pierre Auger Observatory*, PoS(ICRC2019) 231 (2019), doi:10.22323/1.358.0231

[5] A. Aab et al. (Pierre Auger Coll.), *Observation of a large-scale anisotropy in the arrival directions of cosmic rays above 8×10^{18} eV*, Science **357**, 1266 (2017), doi:10.1126/science.aan4338

[6] A. Aab et al. (Pierre Auger Coll.), *Large-scale cosmic-ray anisotropies above 4 EeV measured by the Pierre Auger Observatory*, Astrophys.J. **868**, 4 (2018), doi:10.3847/1538-4357/aae689

[7] A. Abdul Halim et al. (Pierre Auger Coll.), *Large-scale cosmic ray anisotropies with 19 years of data from the Pierre Auger Observatory*, accepted in Astrop.J., arXiv:2408.05292, doi:10.48550/arXiv.2408.05292

[8] P. Abreu et al. (Pierre Auger Coll.), *Arrival Directions of Cosmic Rays above 32 EeV from Phase One of the Pierre Auger Observatory*, Astrop.J. **935**, 170 (2022), doi:10.3847/1538-4357/ac7d4e

[9] G. Golup (Pierre Auger Coll.), *An update on the arrival direction studies made with data from the Pierre Auger Observatory*, PoS(ICRC2023) 252 (2023), doi:10.22323/1.444.0252

[10] J. Kim for the Telescope Array Collaboration, EPJ Web of Conferences 283 (2023) 03005, doi:10.1051/epjconf/202328303005

[11] Pierre Auger Coll. and Telescope Array, *Update on the searches for anisotropies in UHECR arrival directions with the Pierre Auger Observatory and the Telescope Array*, PoS(ICRC2023) 521 (2023), doi:10.22323/1.444.0521

[12] A. Aab et al. (Pierre Auger Coll.), *Measurement of the cosmic-ray energy spectrum above 2.5×10^{18} eV using the Pierre Auger Observatory*, Phys. Rev. D **102**, 6, 062005 (2020), doi:10.1103/PhysRevD.102.062005

[13] P. Abreu et al. (Pierre Auger Coll.), *The energy spectrum of cosmic rays beyond the turn-down around 10^{17} eV as measured with the surface detector of the Pierre Auger Observatory*, Eur.Phys.J. C **81**, 966 (2021), doi:10.1140/epjc/s10052-021-09700-w

[14] G. Brichetto Orquera (Pierre Auger Coll.), *The second knee in the cosmic ray spectrum observed with the surface detector of the Pierre Auger Observatory*, PoS(ICRC2023) 398 (2023), doi:10.22323/1.444.0398

[15] E. Mayotte (Pierre Auger Coll.), *Measurement of the mass composition of ultra-high-energy cosmic rays at the Pierre Auger Observatory*, PoS(ICRC2023) 365 (2023), doi:10.22323/1.444.0365

[16] A. Aab et al. (Pierre Auger Coll.), *Inferences on mass composition and tests of hadronic interactions from 0.3 to 100 EeV using the water-Cherenkov detectors of the Pierre Auger Observatory*, Phys.Rev.D **96**, 122003 (2017), doi:10.1103/PhysRevD.96.122003

[17] T. Fitoussi (Pierre Auger Coll.), *Depth of Maximum of Air-Shower Profiles above 1017.8eV Measured with the Fluorescence Detector of the Pierre Auger Observatory and Mass Composition Implications*, PoS(ICRC2023) 319 (2023), doi:10.22323/1.444.0319

[18] J. Glombitza (Pierre Auger Coll.), *Mass Composition from 3 EeV to 100 EeV using the Depth of the Maximum of Air-Shower Profiles Estimated with Deep Learning using Surface Detector Data of the Pierre Auger Observatory*, PoS(ICRC2023) 278 (2023), doi:10.22323/1.444.0278 (arXiv:2406.06315)

[19] B. Pont (Pierre Auger Coll.), *The depth of the shower maximum of air showers measured with AERA*, EPj Web Conf. **283**, 02010 (2023), doi:10.1051/epjconf/202328302010

[20] A. Abdul Halim et al. (Pierre Auger Coll.), *Constraining the sources of ultra-high-energy cosmic rays across and above the ankle with the spectrum and composition data measured at the Pierre Auger Observatory*, JCAP **2023**, 024 (2023), doi:10.1088/1475-7516/2023/05/024

[21] O. Tkachenko (Pierre Auger Coll.), *Studies of the mass composition of cosmic rays and proton-proton interaction cross-sections at ultra-high energies with the Pierre Auger Observatory*, PoS(ICRC2023) 438 (2023), doi:10.22323/1.444.0438

[22] A. Yushkov (Pierre Auger Coll.), *Mass Composition of Cosmic Rays with Energies above $10^{17.2}$ eV from the Hybrid Data of the Pierre Auger Observatory*, PoS(ICRC2019) 482 (2019), doi:10.22323/1.358.0482

[23] M. Niechciol (Pierre Auger Coll.), *Latest results from the searches for ultra-high-energy photons and neutrinos at the Pierre Auger Observatory*, PoS(ICRC2023) 1488 (2023), doi:10.22323/1.444.1488

[24] C. Petrucci (Pierre Auger Coll.), *Investigating the UHECR characteristics from cosmogenic neutrino limits with the measurements of the Pierre Auger Observatory*, PoS(ICRC2023) 1520 (2023), doi:10.22323/1.444.1520

[25] A. Abdul Halim et al. (Pierre Auger Coll.), *Impact of the Magnetic Horizon on the Interpretation of the Pierre Auger Observatory Spectrum and Composition Data*, JCAP **07**, 094 (2024), doi:10.1088/1475-7516/2024/07/094

[26] A. Abdul Halim et al. (Pierre Auger Coll.), *Constraining models for the origin of ultra-high-energy cosmic rays with a novel combined analysis of arrival directions, spectrum, and composition data measured at the Pierre Auger Observatory*, JCAP **01**, 022 (2024), doi:10.1088/1475-7516/2024/01/022

[27] P. Abreu et al. (Pierre Auger Coll.), *Measurement of the p-Air cross-section at $\sqrt{s} = 57$ TeV with the Pierre Auger Observatory*, Phys.Rev.Lett. **109**, 062002 (2012), doi:10.1103/PhysRevLett.109.062002

[28] A. Aab et al. (Pierre Auger Coll.), *Muons in air showers at the Pierre Auger Observatory: Mean number in highly inclined events*, Phys.Rev.D **91**, 032003 (2015), doi:10.1103/PhysRevD.91.032003

[29] A. Aab et al. (Pierre Auger Coll.), *Testing Hadronic Interactions at Ultrahigh Energies with Air Showers Measured by the Pierre Auger Observatory*, Phys. Rev. Lett. 117 192001 (2016) doi:10.1103/PhysRevLett.117.192001.

[30] A. Aab et al. (Pierre Auger Coll.), *Direct measurement of the muonic content of extensive air showers between 2×10^{17} eV and 2×10^{18} eV at the Pierre Auger Observatory*, Eur.Phys.J.C **80**, 751 (2020), doi:10.1140/epjc/s10052-020-8055-y

[31] A. Aab et al. (Pierre Auger Coll.), *Measurement of the Fluctuations in the Number of Muons in Extensive Air Showers with the Pierre Auger Observatory*, Phys.Rev.Lett. **126**, 152002 (2021), doi:10.1103/PhysRevLett.126.152002

[32] A. Abdul-Halim et al. (Pierre Auger Coll.), *Testing Hadronic-Model Predictions of Depth of Maximum of Air-Shower Profiles and Ground-Particle Signals using Hybrid Data of the Pierre Auger Observatory*, Phys.Rev.D **109**, 101001 (2024), doi:10.1103/PhysRevD.109.102001

[33] J. Matthews, A Heitler model of extensive air showers, Astropart. Phys. 22, 387 (2005), doi:10.1016/j.astropartphys.2004.09.003

[34] P. Abreu et al. (Pierre Auger Coll.), *Testing effects of Lorentz invariance violation in the propagation of astroparticles with the Pierre Auger Observatory*, JCAP **01**, 023 (2022), doi:10.1088/1475-7516/2022/01/023

[35] C. Trimarelli (Pierre Auger Coll.), *Constraining Lorentz Invariance Violation using the muon content of extensive air showers measured at the Pierre Auger Observatory*, PoS(ICRC2021) 340 (2021) doi:10.22323/1.395.0340

[36] P. Abreu et al. (Pierre Auger Coll.), *Limits to gauge coupling in the dark sector set by the non-observation of instanton-induced decay of Super-Heavy Dark Matter in the Pierre Auger Observatory data*, Phys. Rev. Lett. 130 (2023) 06100, doi:10.1103/PhysRevLett.130.061001

[37] P. Abreu et al. (Pierre Auger Coll.), *Constraints on metastable superheavy dark matter coupled to sterile neutrinos with the Pierre Auger Observatory*, Phys.Rev.D **109**, L081101 (2024), doi:10.1103/PhysRevD.109.L081101

[38] A. Castellina (Pierre Auger Coll.), *AugerPrime: the Pierre Auger Observatory Upgrade*, EPJ Web of Conf. **210**, 06002 (2019), doi:10.1051/epjconf/201921006002

[39] F. Convenga (Pierre Auger Coll.), *The performances of the upgraded surface detector stations of AugerPrime*, PoS(ICRC2023) 392 (2023), doi:10.22323/1.444.392

[40] G. Anastasi (Pierre Auger Coll.), *The dynamic range of the upgraded surface detector stations of AugerPrime*, PoS(ICRC2023) 343 (2023), doi:10.22323/1.444.343

[41] R. Sato (Pierre Auger Coll.), *AugerPrime implementation in the DAQ systems of the Pierre Auger Observatory*, PoS(ICRC2023) 373 (2023), doi:10.22323/1.444.373

[42] J. de Jesus (Pierre Auger Coll.), *Status and Performance of the Underground Muon Detector of the Pierre Auger Observatory*, PoS(ICRC2023) 267 (2023), doi:10.22323/1.444.267

[43] J. Pawlowsky (Pierre Auger Coll.), *Status and expected performance of the AugerPrime Radio Detector*, PoS(ICRC2023) 344 (2023), doi:10.22323/1.444.344